We are IntechOpen,
the world's leading publisher of
Open Access books
Built by scientists, for scientists

4,800
Open access books available

122,000
International authors and editors

135M
Downloads

Our authors are among the

154
Countries delivered to

TOP 1%
most cited scientists

12.2%
Contributors from top 500 universities

BOOK CITATION INDEX
CLARIVATE ANALYTICS
INDEXED

WEB OF SCIENCE™

Selection of our books indexed in the Book Citation Index
in Web of Science™ Core Collection (BKCI)

Interested in publishing with us?
Contact book.department@intechopen.com

Numbers displayed above are based on latest data collected.
For more information visit www.intechopen.com

Chapter

Atomic Scale Magnetic Sensing and Imaging Based on Diamond NV Centers

Myeongwon Lee, Jungbae Yoon and Donghun Lee

Abstract

The development of magnetic sensors simultaneously satisfying high magnetic sensitivity and high spatial resolution becomes more important in a wide range of fields including solid-state physics and life science. The nitrogen-vacancy (NV) center in diamond is a promising candidate to realize nanometer-scale magnetometry due to its excellent spin coherence properties, magnetic field sensitivity, atomic-scale size and versatile operation condition. Recent experiments successfully demonstrate the use of NV center in various sensing and imaging applications. In this chapter, we review the basic sensing mechanisms of the NV center and introduce imaging applications based on scanning magnetometry and wide field-of-view optics.

Keywords: magnetic sensor, diamond NV center, quantum sensing, scanning magnetometry, wide field-of-view optics

1. Introduction

Understanding magnetic properties at the microscopic level plays an important role in the development of modern science and technology [1, 2]. For instance, writing and reading information using nanometer size magnetic bits is the heart of massive data storage indispensable in the modern information technology [1]. Magnetic resonance imaging (MRI) which is an important medical tool of imaging the inner structures of human body is also based on sensing the magnetic response of minuscule protons with respect to radio frequency (RF) electromagnetic waves [2]. For fundamental research, on the other hand, studying magnetic phases and spin textures at the nanometer scale are one of the hottest topics in solid-state physics due to the recent discovery of exotic materials and topological phases [3–5]. Therefore, it is not too much to say that the continuous advances in modern science and technology strongly reply on the precise sensing and control of magnetism at the atomic level.

The paradigm of modern science and technology seems to shift from charge-based devices to spin-based systems. Nonetheless studying spins is a lot more difficult than electric charges mainly due to the lack of sensitive measurement techniques of magnetic field. For instance, the size of magnetic bits used in MOSFET (Metal-Oxide-Semiconductor Field-Effect Transistor) and STT-MRAM (Spin-Transfer Torque Magnetic Random-Access Memory) are less than 10

nanometers and eventually reaches at the level of single spins requiring sensitive detection of individual spins with high spatial resolution [6, 7]. However, detecting single electron spin takes more than 13 hours even with the best magnetometer [8], while sensing single electron charge takes only 1 picosecond [9, 10]. This motivates to develop new magnetic sensors with high magnetic field sensitivity and high spatial resolution.

Existing magnetometers are insufficient to satisfy both requirements especially when trying to measure minute magnetic fields at the length scale of 100 nm or below. For instance, SQUID (Superconducting Quantum Interference Devices), atomic vapor cell and Hall bar are very sensitive magnetometers but their spatial resolutions are typically limited to tens of micrometers [11, 12]. On the other hand, scanning probe type tools such as SP-STM (Spin-Polarized Scanning Tunneling Microscope) and MFM (Magnetic Force Microscope) exhibit very high spatial resolution but their sensitivity is relatively low and not quantitatively defined [13, 14]. Moreover, magnetic films coated at the tips may produce unwanted stray field affecting the magnetic samples to be measured.

Here, we introduce a novel magnetometer enabling non-invasive, extremely sensitive magnetic sensing and imaging at the nanometer scale. It is based on diamond NV (nitrogen-vacancy) center which is an atomic size point defect in the diamond crystal providing high spatial resolution. It is also a spin qubit (i.e. quantum bit) possessing remarkable magnetic and quantum properties satisfying high field sensitivity [15, 16]. Since it can also operate over a wide range of temperature from room temperature down to cryogenic temperatures and is chemically inert and non-toxic, the NV center already has been applied in various experiments including magnetic imaging of solid-state materials and biomedical samples [17, 18]. In this chapter, we will discuss basic working principles of diamond NV centers (Section 2) and their sensing mechanisms (Section 3). Furthermore, we will provide two examples of imaging applications; scanning probe type imaging (Section 4.1) and wide field-of-view optical imaging (Section 4.2) (**Figure 1**).
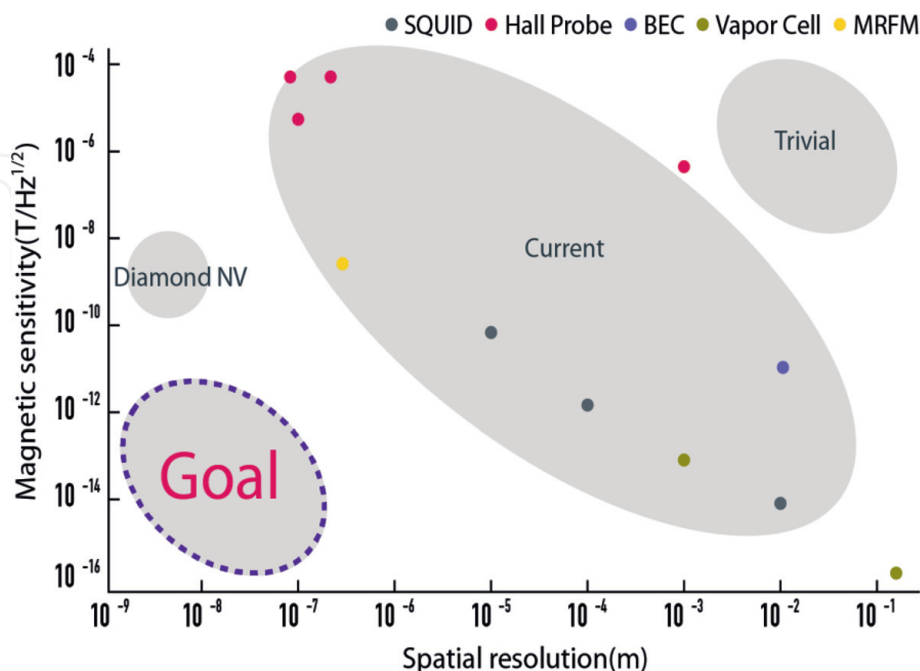

Figure 1.
Comparison of various magnetometers in terms of spatial resolution and magnetic field sensitivity. The diamond NV center is a promising candidate to realize the goal of highly sensitive sensing with nanometer-scale resolution. The data are adopted from [36]; MRFM[8]; SQUID [38–40]; Hall probe [41, 42]; BEC 43; Vapor Cell [44].

2. Background of diamond NV center

The diamond NV center is a hetero-molecular defect in a diamond crystal consisting of a substitutional nitrogen defect combined with an adjacent carbon vacancy [15, 16] (**Figure 2a**). It is a color center as it absorbs photons in the visible range of wavelength (e.g. 532 nm) and emits photons of a broad range of wavelength (e.g. 632–800 nm). The NV center can exist in a natural diamond, but it can be created in more controllable fashion, for instance, by implanting nitrogen ions into the diamond. Subsequent high temperature annealing (e.g. at 800°C) results in the thermal migration of carbon vacancies and NV centers are formed once the vacancies meet the implanted nitrogen impurities. The density and location of NV centers in diamond are well controlled with various techniques. **Figure 2b** shows an example of precise positioning of NV centers less than a few hundred of nanometers uncertainty [19].

When negatively charged, the NV center has total six electrons (i.e. three electrons from three carbons, two electrons from the substitutional nitrogen and one electron from the diamond lattice). Four of them form pairs and the remaining two unpaired electrons make spin triplet states (i.e. S = 1) in the ground energy level. The spin triplet states are split into $m_s = 0$ and $m_s = \pm 1$ whose separation is about 2.9 GHz at room temperature due to the crystal field and spin–spin interaction [17, 18] (this is called zero-field splitting). As shown in **Figure 3a**, the degenerated $m_s = \pm 1$ states are split further if there is non-zero magnetic field along the NV crystal axis (i.e. the quantized axis of NV spin). Sensing magnetic field (i.e. magnetic field component along the NV axis) is realized by measuring the amount of Zeeman splitting [17, 18] (e.g. 5.6 MHz splitting per 1 Gauss field).

The optical response of the NV center varies depending on its spin states. When it is in the $m_s = 0$ state, almost 100% cycling transition occurs upon optical pumping. On the other hand, for the case of $m_s = \pm 1$ states, 10–30% of the excited electrons undergo intersystem crossing (ISC) to the spin singlet states and relax into the $m_s = 0$ ground state. This dark transition results in the reduction of the number of emitted photons relative to the $m_s = 0$ state. Furthermore, the transition via the shelving states produces spin flip from the $m_s = \pm 1$ states to the $m_s = 0$ state. The spin-sensitive fluorescence and spin-flip transition allow optical readout of the spin states as well as optical initialization of the qubit state [15–18].

The energy levels of NV center are located well within the bandgap of diamond (i.e. 5.3 eV) making it effectively isolated from the hosting material and enabling to preserve its intrinsic quantum properties. Thus, the NV center has exceptionally long spin coherence times even at room temperature [20] (e.g. $T_2 > 1$ ms). In
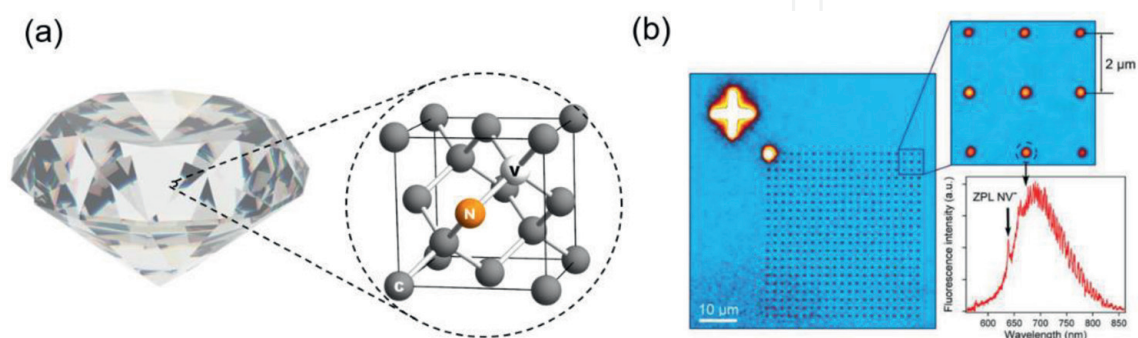

Figure 2.
Physical properties of diamond NV center. (a) Crystal structure of NV center in a diamond lattice. NV center consists of nitrogen substitutional defect and carbon vacancy. (b) Precise formation of NV centers using focused ion beam (FIB) implantation of nitrogen. Reprint with permission from [19]. Copyright (2013) Wiley-VCH Verlag GmbH & Co. KGaA. Reproduced with permission.
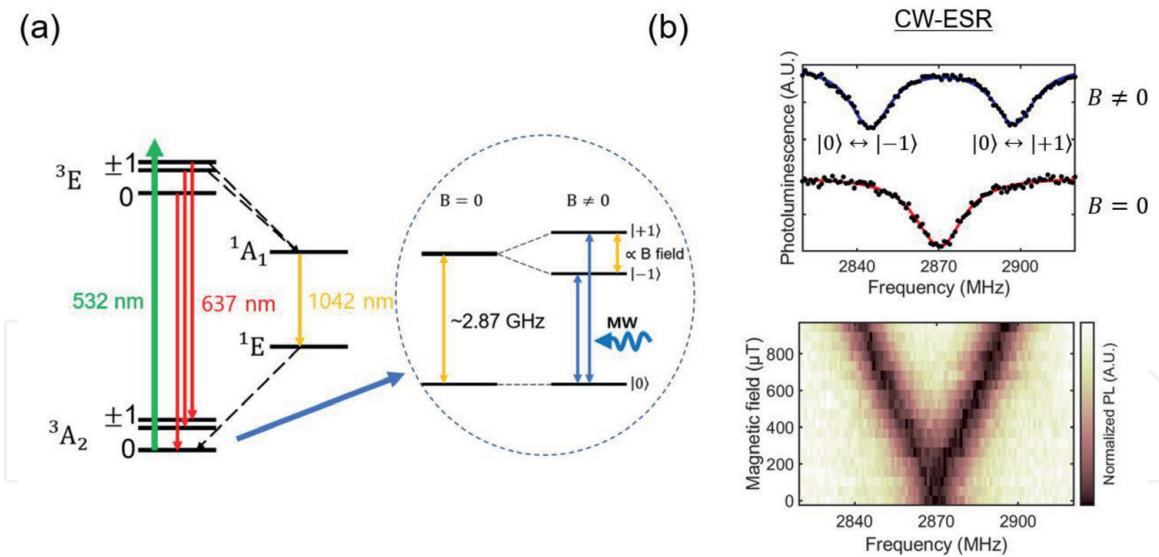
Figure 3.
Electronic properties of diamond NV center. (a) Energy levels and optical transitions are illustrated. The spin triplet ground states are used to realize a spin qubit for the magnetic field sensing. (b) Photoluminescence signal as a function of microwave frequency reveals the Zeeman splitting providing information about the external magnetic field. This method is called CW-ESR measurement.

addition, the NV spin is highly sensitive to various fields, including temperature, magnetic, electric and strain fields [18]. For example, the magnetic field sensitivity for a single NV center is on the order of $1 \, \text{nT}/\sqrt{\text{Hz}}$ which is about 10^5 smaller than typical earth magnetic field [16–18]. Higher sensitivity can be also possible using either NV ensembles [21] (e.g. $<1 \, \text{pT}/\sqrt{\text{Hz}}$) or advanced sensing protocols [22]. The high magnetic field sensitivity is one of the key ingredients of realizing novel magnetometer introduced in this chapter.

3. Sensing mechanism

In this section, we will discuss various sensing methods specifically designed to study magnetism in different spectral regimes from static spin distributions to high frequency magnetic excitations. Sections 3.1 and 3.2 elucidate basic mechanisms used for sensing static and dynamic magnetic fields. The section ends with a brief outlook on advanced sensing techniques (Section 3.3).

3.1 Sensing dc magnetic field

Probing static field from magnetic textures or current flow in transport devices is an important capability to study microscopic magnetism in condensed matter physics. The diamond NV centers already have been used to study a diverse set of magnetic systems including skyrmions [23], superconducting vortices [24, 25], domain walls [26], magnetic nanowires [27], and steady-state current distributions in graphene [28]. Various experimental methods have been implemented to detect static dc magnetic field and we will examine the two most common protocols; continuous wave electron spin resonance (CW-ESR) and Ramsey interferometry.

As seen in **Figure 3b**, the ground spin states of NV center are subject to change by external magnetic field via the Zeeman effect. Upon continuous illumination of the pumping laser and gigahertz microwave photons, ESR transitions of $m_s = 0 \leftrightarrow m_s = -1$ and $m_s = 0 \leftrightarrow m_s = +1$ occurs. The ESR signals appear as negative peaks in the photoluminescence (PL) measurement due to the dark transitions

associated with the $m_s = \pm 1$ states. Since the ESR spectrum is obtained by optical means, this method is often called as optically detected magnetic resonance (ODMR).

The amount of dc magnetic field is extracted from the ESR splitting of $\Delta f = 2\gamma B_{NV}$, where Δf is the frequency difference of the two transitions, γ is the gyromagnetic ratio (i.e. 2.8 MHz/G) and B_{NV} is the magnetic field along the NV axis. The CW-ESR signal can be analyzed by fitting the spectrum with a Lorentzian peak,

$$I(f) = I_0 \left(1 - C \frac{(f_{FWHM}/2)^2}{(f - f_0)^2 + (f_{FWHM}/2)^2} \right) \qquad (1)$$

where I_0 is the photon count rate, C is the optical contrast between the spin states, f_0 is the ESR central frequency, and f_{FWHM} is the full width half maximum of the resonance. The sensitivity of dc magnetic field based on this method is determined by the minimum resolvable frequency shift (**Figure 4**) which is defined as $\Delta f = \frac{\Delta N}{\partial N / \partial f}$, where N is total number of photons during the measurement time, T, i.e. $N = I(f)T$. For the shot noise limited photon measurement, $\Delta N \approx \sqrt{N}$ and the minimum detectable magnetic field and the sensitivity become [16].
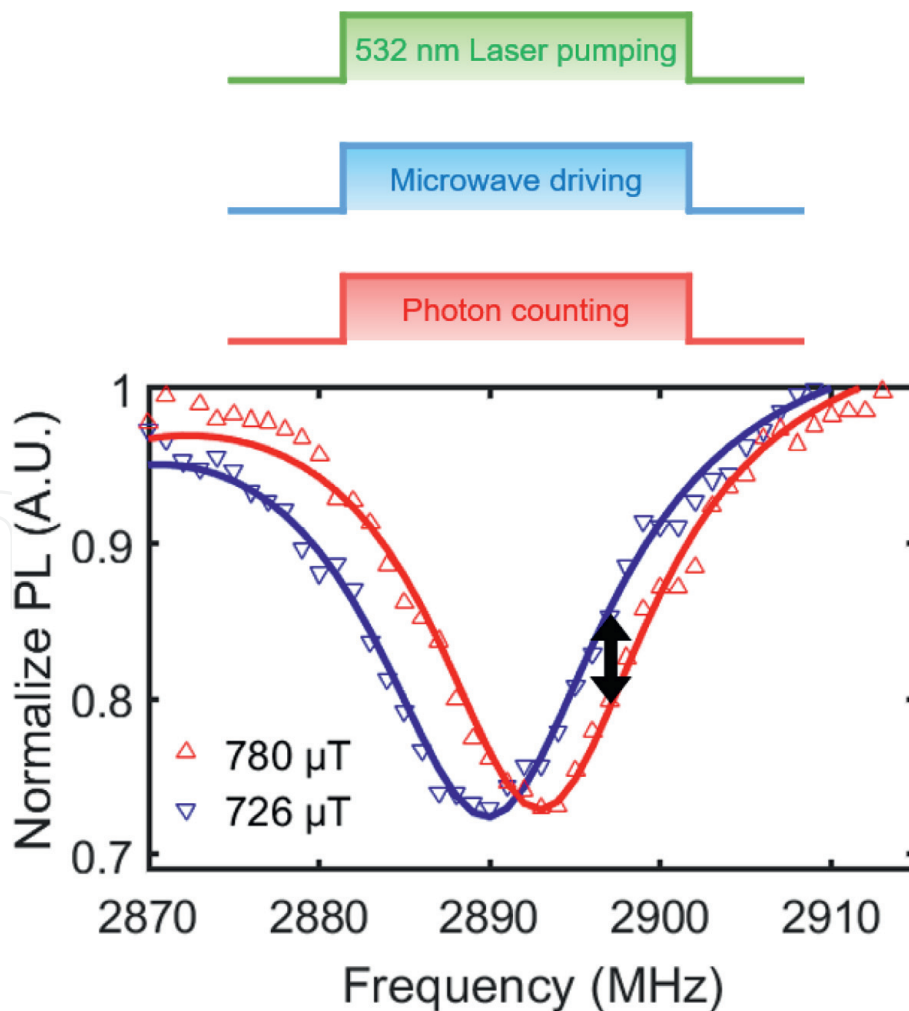

Figure 4.
Sensing dc magnetic field based on CW-ESR measurement. Continuous wave of laser and microwave photons are used. The shift in frequency gives an information about the magnitude and direction of external magnetic field.

$$B_{min} = \frac{\Delta f}{\gamma} \approx \frac{\sqrt{I_0 T}}{\gamma C I_0 T / f_{\text{FWHM}}} = \frac{f_{\text{FWHM}}}{\gamma C \sqrt{I_0 T}}, \quad \eta_B = B_{min} \sqrt{T} \approx \frac{f_{\text{FWHM}}}{\gamma C \sqrt{I_0}}. \tag{2}$$

As seen in Eq. (2), the sensitivity is limited by the ESR linewidth and in principle it can be as narrow as the inverse of NV's inhomogeneous dephasing time, T_2^*. However, practical linewidth suffers from the power broadening due to continuous laser and microwave excitation. Therefore, typical magnetic sensitivity based on CW-ESR is limited to on the order of $1 \, \mu T / \sqrt{\text{Hz}}$.

The power broadening problem can be avoided by using pulsed laser and microwave photons. Ramsey interferometry is one of the basic pulse techniques used to measure the free induction decay of a spin qubit. **Figure 5a** shows Ramsey pulse sequences used in the NV measurement. The two laser pulses are used for optical initialization and readout while the two $\pi/2$ microwave pulses are used to make qubit superposition state and to project it back to the initial state. The basic idea of Ramsey interferometry is very similar with Michelson interferometry. The first laser pulse polarizes the NV center to the $m_s = 0$ state and the subsequent $\pi/2$ microwave pulse rotates the spin into the equal superposition of $m_s = 0$ and $m_s = +1$ (or $m_s = -1$) state. This works as a 50:50 beam splitter used in the Michelson interferometry experiment. Under external magnetic field, the two spin states evolve together but with different phases each other and the amount of accumulated phase depends on the magnitude of dc field. If the microwave frequency is detuned from the qubit energy by δ, the Ramsey signal oscillates at the frequency of δ and is written as

$$I(t) \approx I_0 \left(1 - \frac{C}{2} \right) + I_0 \frac{C}{2} \left(e^{-\left(\frac{t}{T_2^*}\right)^2} \cos \delta t \right) \tag{3}$$
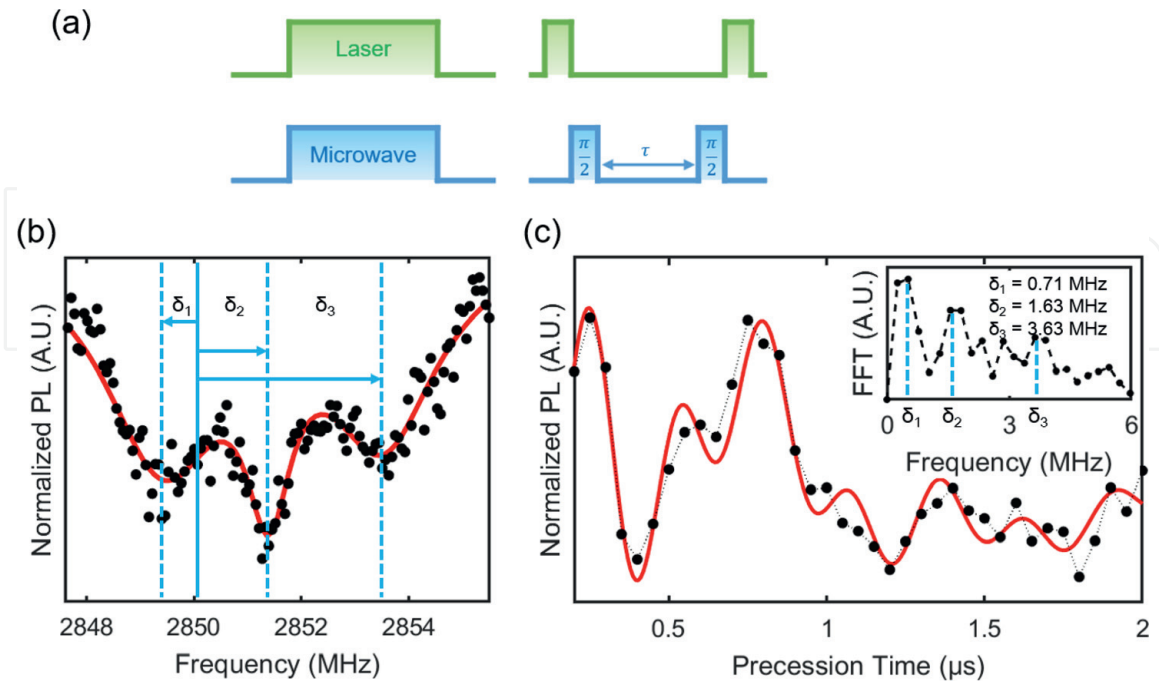

Figure 5.
Sensing dc magnetic field based on Ramsey interferometry. (a) Schematics of laser and microwave pulse used for the measurement. (b) A close view of the resonance peak in CW-ESR reveals three sub-features resulting from the NV's hyperfine coupling with ^{14}N nuclear spin. (c) Ramsey measurement with the detunings in (b) shows the beatings of three oscillations. Subset presents the FFT of the Ramsey signal showing three peaks corresponding to the detunings.

where t is the free induction time. Shift in the oscillation frequency gives the information about static magnetic field and the resolvable frequency shift is now limited by T_2^*. The minimum detectable magnetic field and the sensitivity are written as.

$$B_{min} = \frac{\Delta\delta}{\gamma} \approx \frac{\sqrt{I_0 t_r n}}{\gamma C I_0 t_r n t} e^{\left(\frac{t}{T_2^*}\right)^2}, \, \eta_B \approx B_{min}\sqrt{n(t_r+t)} \approx B_{min}\sqrt{nt} = \frac{1}{\gamma C\sqrt{I_0 t_r}\sqrt{T_2^*}} \approx \frac{1}{\sqrt{T_2^*}}$$

(4)

where t_r is the single shot readout time (e.g. a few hundreds of nanoseconds) and n is the total number of measurement cycles [16]. Based on this method, the dc field sensitivity from a single NV center can be as high as $\eta_B \sim 10$ nT/$\sqrt{Hz}$ for $T_2^* \sim 100$ μs [16].

Figure 5b and **c** shows an example of the Ramsey measurement. The ESR resonance exhibits three hyperfine structures due to the dipole-dipole interaction between NV electron spin and ^{14}N nuclear spin (I = 1). Therefore, the beatings of three oscillations appear in the Ramsey signal (**Figure 5c**) which is defined as,

$$I(t) = I_0\left(1 - \frac{C}{2}\right) + I_0\frac{C}{2}\left(e^{-\left(\frac{t}{T_2^*}\right)^2}\frac{1}{3}\sum_i^3 \cos\left(\delta_i t + \phi_i\right)\right)$$

(5)

where δ_i ($i = 1, 2, 3$) are the detunings of three hyperfine levels and ϕ_i are the phase offsets. The fast Fourier transformation (FFT) of the signal also reveals three frequencies (subset in **Figure 5c**) whose shifts are used to probe static field.

3.2 Sensing ac magnetic field

The NV center can also detect ac magnetic field up to gigahertz. The large bandwidth sensing capability is important to study spin dynamics in solid-state systems and biological samples. For example, nuclear spin precession in biomolecules occurs at 100 kHz–MHz regime while spin excitations or charge fluctuations in solids happen at higher frequency of MHz–GHz [22]. Various sensing methods with its detection bandwidth are listed in **Figure 6** and, in this section, we will
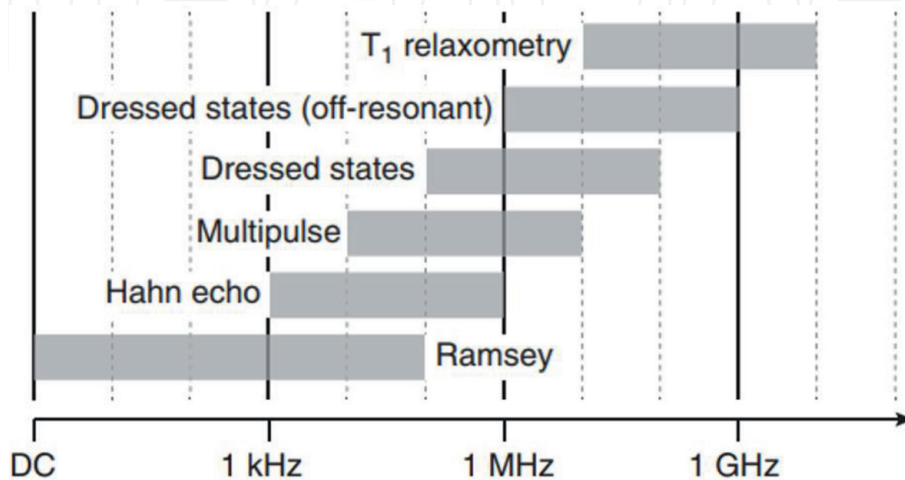

Figure 6.
Detection bandwidth of various sensing methods. NV center can measure magnetic field from dc to gigahertz ac frequency. Reprint with permission from Ref. [22]. Copyright (2017) Reviews of Modern Physics.
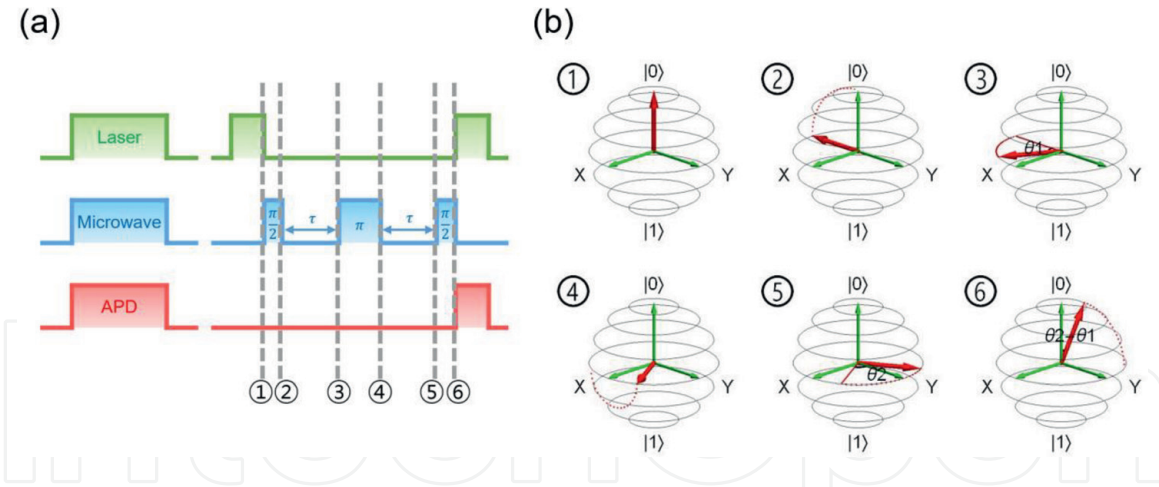
Figure 7.
Sensing ac magnetic field based on spin Hahn echo measurement. (a) Schematics of the Hahn echo pulses. (b) Bloch representations of the spin status according to the numbers indicated in (a).

explain two basic dynamical decoupling methods such as spin Hahn echo and Carr-Purcell-Meiboom-Gill (CPMG).

Spin Hahn echo measurement consists of a similar pulse sequence as Ramsey interferometry but having an extra π pulse in the middle of the sequence (**Figure 7a**). This additional pulse flips the sign of accumulated phase during the free induction evolution resulting in the cancelation of dc and low frequency magnetic field. When the pulse duration matches to the period of ac magnetic field, however, the phase survives and continues to be accumulated. In this way, one can selectively probe ac magnetic field.

This can be better viewed with the Bloch sphere representation shown in **Figure 7b**. In the rotating frame at the qubit frequency, the spin rotates around the equator by an angle, θ, which is determined by the free precession time, τ, between $\pi/2$ and π pulses (② and ⑤ in **Figure 7b**). The angles from the first (②) and the second period (⑤) of the echo pulse are written as,

$$\theta_1 = \int_0^\tau \gamma B_{AC} \sin(\omega t' + \alpha)dt', \; \theta_2 = \int_\tau^{2\tau} \gamma B_{AC} \sin(\omega t' + \alpha)dt' \tag{6}$$

where B_{AC} is the amplitude of ac magnetic field and α is a phase offset. And their difference is

$$\theta_2 - \theta_1 = \frac{4\gamma B_{AC}}{\omega} \cos(\omega\tau + \alpha) \sin^2 \frac{\omega\tau}{2} \tag{7}$$

This difference determines the projected probability of the qubit and becomes non-zero if the sign of B_{AC} flips before and after the π pulse. The probabilities of the $|0\rangle$ and $|1\rangle$ states after a single echo sequence are obtained as,

$$P_{|1\rangle} = \sin^2\left(\frac{\theta_2 - \theta_1}{2}\right), \; P_{|0\rangle} = \cos^2\left(\frac{\theta_2 - \theta_1}{2}\right). \tag{8}$$

Finally, an average probability of the qubit state after repeated Hahn echo cycles (but with random phase offset, α) can be expressed as the first order Bessel function,

$$P_{|0\rangle, \text{avg}} = \frac{1}{2\pi} \int_{-\pi}^{\pi} \cos^2\left[\frac{2\gamma B_{AC}}{\omega} \cos(\omega\tau + \alpha) \sin^2 \frac{\omega\tau}{2}\right] d\alpha = \frac{1}{2}\left[1 + J_0\left(\frac{4\gamma B_{AC}}{\omega} \sin^2 \frac{\omega\tau}{2}\right)\right]. \tag{9}$$
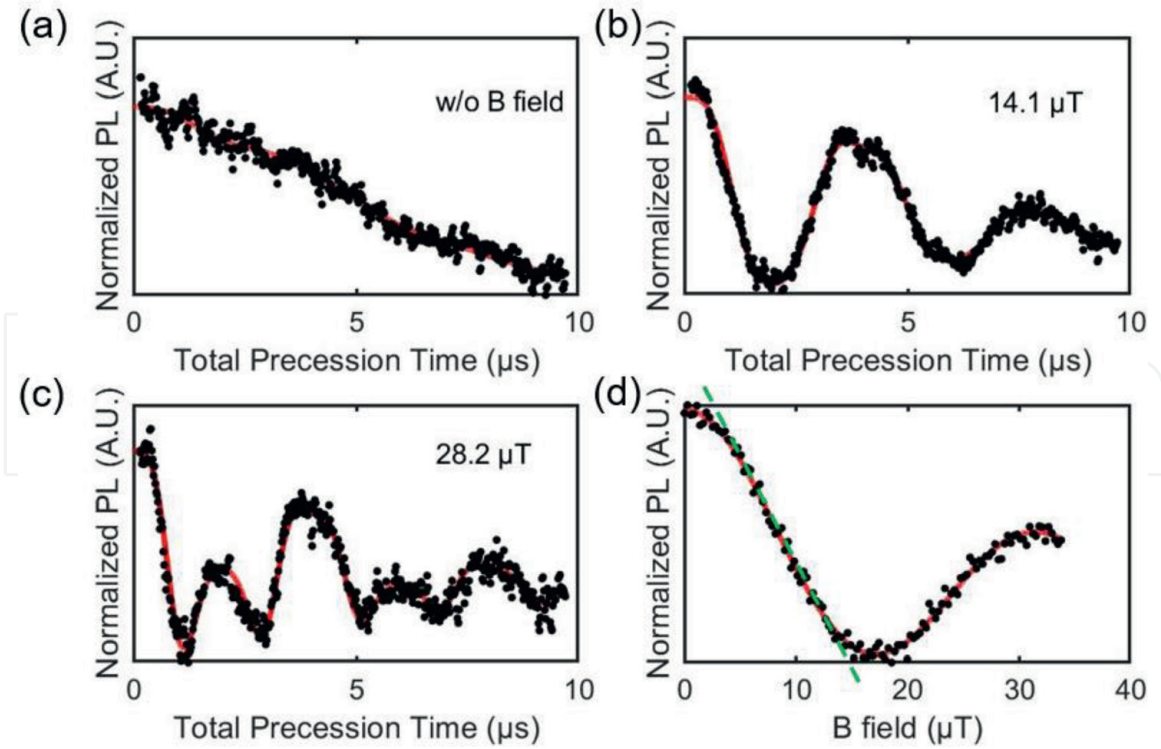
Figure 8.
Examples of the Hahn echo measurement as a function of ac field strength. (a–c) Hahn echo signals with various strengths of ac magnetic field at 500 kHz. (a) no field, (b) 14.1 μT, and (c) 28.2 μT. (d) Hahn echo signals as a function of the magnetic field strength measured at $2\tau = 2$ μs. Minimum detectable magnetic field of $B_{min} = 0.84 \pm 0.02$ μT is obtained from the dashed line of the maximum slope.

Figure 8 shows an example of the spin Hahn echo measurement as a function of the free precession time, τ, and the ac field strength, B_{AC}. For the experiment, external field at 500 kHz frequency is applied with a wire. Compared to a monotonic exponential decay in **Figure 8a**, the first order Bessel functions discussed in Eq. (9) are clearly observed for the cases of non-zero ac fields (**Figure 8b** and **c**). The field sensitivity can be determined from the maximum change of the PL signal with respect to B_{AC}. For instance, **Figure 8d** shows the normalized PL as a function of B_{AC} measured at the time, $2\tau = 2$ μs. The minimum detectable field (or sensitivity) is obtained from the ratio of the maximum slope over the noise level in the PL signal (shot noise limited in this measurement) which is $B_{min} = 0.84 \pm 0.02$ μT at 500 kHz.

By adding more periodic microwave pulses in the sequence, one can extend the spin coherence time and realize improved sensitivity. For example, CPMG sequence utilizes n pairs of two π pulses separated by 2τ (**Figure 9**) which prolong the spin coherence by $T_2 \propto n^{2/3}$. The axis of π pulse can be also alternated between x and y in the Bloch sphere which can mitigate potential pulse error. Such dynamical decoupling sequences are called XY4 or XY8.

The ac field sensitivity is similar as the dc field sensitivity in Eq. (4) but now the intrinsic spin dephasing time, T_2, limits the sensitivity i.e. $\eta_{B,AC} \approx \eta_{B,DC} \sqrt{\frac{T_2^*}{T_2}}$. The ac field sensitivity based on as a single NV center can be as high as $\eta_B \sim 1\ nT/\sqrt{Hz}$ for $T_2 \sim 1$ ms [16].

3.3 Current limitations and advanced sensing protocols

In general, the bandwidth of dynamical decoupling methods is limited to $\sim$ 10 MHz (**Figure 6**). Higher frequency ac field ($\sim$GHz) can be measured by T_1
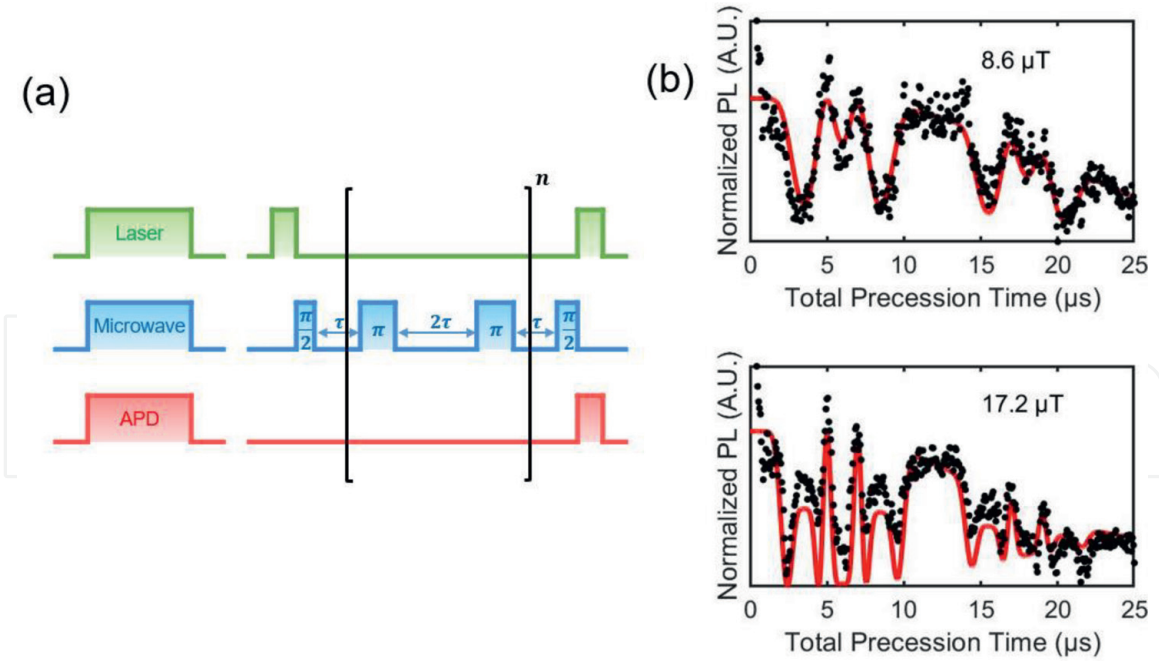
Figure 9.
Sensing ac magnetic field based on CPMG measurement. (a) Schematics of the CPMG pulses. (b) CPMG signals with two different ac magnetic fields at 500 kHz, i.e. 8.6 and 17.2 μT.
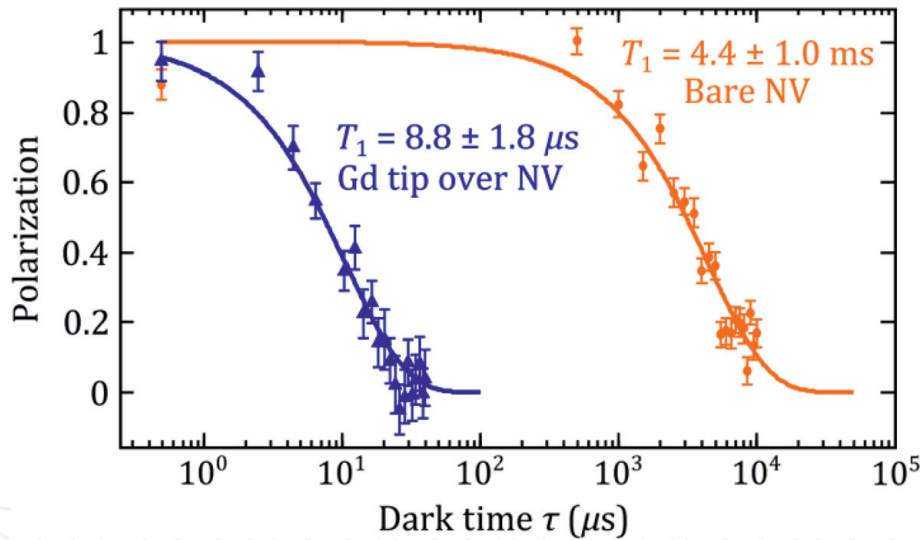

Figure 10.
An example of T$_1$ relaxometry. Fast fluctuation of Gd³⁺ spins results in the reduction of NV's T$_1$ time enabling sensing of gigahertz frequency ac field. Reprint with permission from Ref. [29]. Copyright (2014) Physical Review Applied.

relaxometry [18, 22]. Dynamic field fluctuation around the qubit frequency can directly affect the qubit relaxation time which can be measured by the relaxometry technique. For instance, **Figure 10** shows that gigahertz spin fluctuations of Gd^{3+} ions result in much faster relaxation of the qubit [29].

In terms of the field sensitivity, higher sensitivity can be realized using either ensembles of NV center or advanced sensing protocols. The former is possible since the sensitivity is proportional to $\sqrt{N}$ where N is the number of NV centers. For instance, sub-picotesla sensitivity has been demonstrated based on an ensemble of $N \sim 10^{11}$ NV centers [21]. The latter relays on advanced sensing methods utilizing various quantum techniques such as sensing assisted by entanglement or auxiliary qubits [22]. For example, nuclear spins typically exhibit 1000 times longer
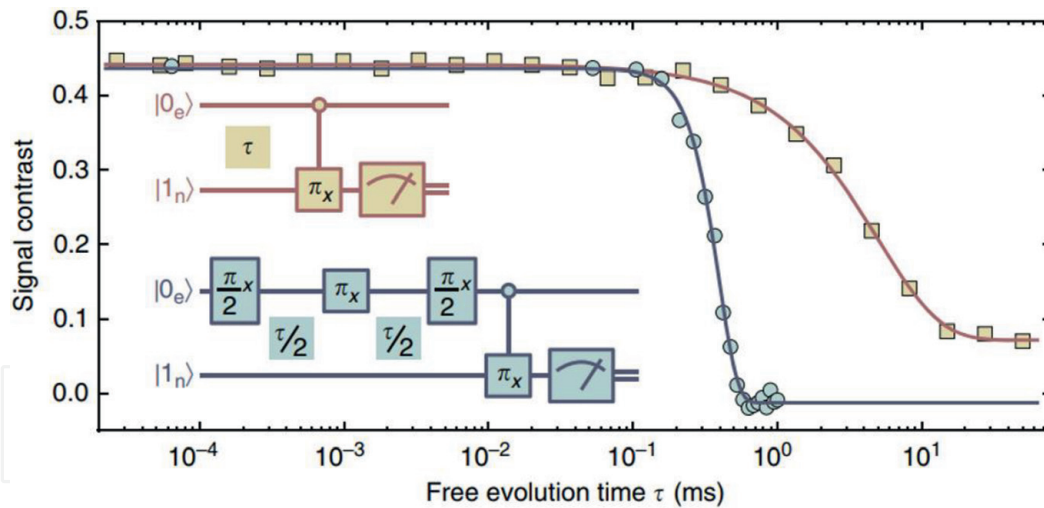
Figure 11.
An example of quantum memory measurement. Spin coherence time is extended by using a neighboring nuclear spin as a memory qubit. Reprint with permission from [30]. Copyright (2016) Nature Communications.

coherence time compared to electron spins such NV center. By using a nuclear spin as an auxiliary qubit via entanglement with the NV electron spin, one can realize extended coherence time and obtain enhanced sensitivity. This method is called quantum memory and an example is shown in **Figure 11** [30].

4. Imaging applications

In this section, we will introduce magnetic imaging techniques based on the diamond NV center. The combined properties of atomic-scale size and high field sensitivity make the NV center as a novel imaging tool to study nanoscale magnetism in the field of condensed matter physics and biology. Multiple imaging techniques have been implemented in several experiments and we will discuss two examples of the diamond imaging techniques; scanning magnetometry and wide field-of-view optics.

4.1 Scanning magnetometry for solid-state systems

Scanning probe microscopy (SPM) is a versatile tool to image sample surface with high spatial resolution. The probe tip can scan over the surface with nanometer step size while maintaining vertical distance with feedback techniques. Scanning tunneling microscope (STM) and atomic force microscope (AFM) are the most common SPM methods used in various experiments. In NV-based imaging applications, different geometries of SPM are possible depending on the position of NV center either on tip or on surface. For example, magnetic molecules that are attached at the end of AFM tip are scanned over a bulk diamond surface where NV centers are located underneath the surface [29] (e.g. 5–20 nm). On the other hand, the NV center can be positioned at the apex of AFM tip and is scanned over magnetic samples [23–26]. There are several benefits of the former geometry. A simple SPM design is possible and there are no needs for complicated diamond fabrication. Moreover, one can use NV centers in a bulk diamond which typically possess good coherence properties. However, this method is not suitable to image large area of sample since it is not easy to be prepared on the tip. Therefore, the geometry of NV-on-tip is more suitable to study solid-state materials.
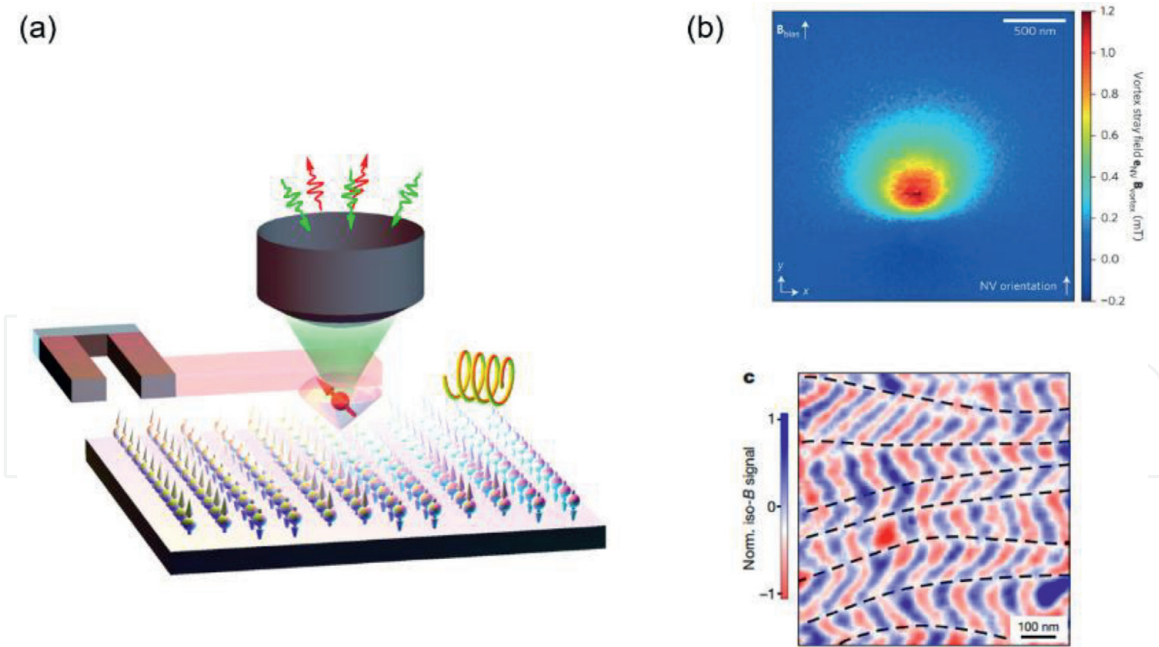
Figure 12.
Scanning magnetometry based on diamond NV center. (a) A schematic of diamond scanning magnetometer. A diamond probe scans over a magnetic sample while an objective lens collects NV photons and a wire produces microwave excitations. (b) Examples of magnetic imaging on various magnetic samples such as superconducting vortex, multiferroic magnetic orders (following from the top image to the bottom image). Reprint with permissions from [31] Copyright (2017) Nature, [24] Copyright (2017) Nature Nanotechnology.

Figure 12a shows a schematic of the NV-on-tip geometry. A fabricated diamond probe with pillar structures or a diamond nano-particle is glued at the end of an AFM tuning fork. An objective lens focuses on the NV center at the tip apex for the optical excitation and readout. A scanning stage maneuvers the sample in three dimensional directions with nanometer step size. In this way, the NV center can effectively scan over the sample and detects local magnetic fields at every scan position on the surface. **Figure 12b** shows examples of the scan images on various magnetic samples including superconducting vortex [24, 25], and multiferroic materials [31]. Since the NV center can operate from room temperature down to cryogenic temperatures, this novel method provides an efficient way to study temperature-dependent evolution of magnetic orders in exotic materials.

4.2 Wide field-of-view optics for life science

The diamond SPM method provides high resolution imaging but is quite slow due to the scanning process (e.g. a few hours per image) and is not an efficient method to study dynamical features. Fast magnetic imaging can be realized by simultaneous mapping the sample with wide field-of-view optics. While confocal optics used in the SPM collects photons only from a focused spot, wide field-of-view optics records optical signals from every point within the optical field-of-view (e.g. $100 \times 100 \ \mu m$) with a CCD (Charge-coupled device) camera. Even though the spatial resolution is not as good as the SPM methods and is diffraction limited, the faster imaging capability gives more advantages when one studies biological samples.

In the diamond wide field-of-view optics experiment, ensembles of NV center are typically used to enhance the field sensitivity and biological samples are placed on a bulk diamond containing NV ensembles. Simultaneous excitation of a number group of NV centers within the field-of-view requires high power of pumping laser. In order to avoid potential damage to the bio-sample due to the high power laser
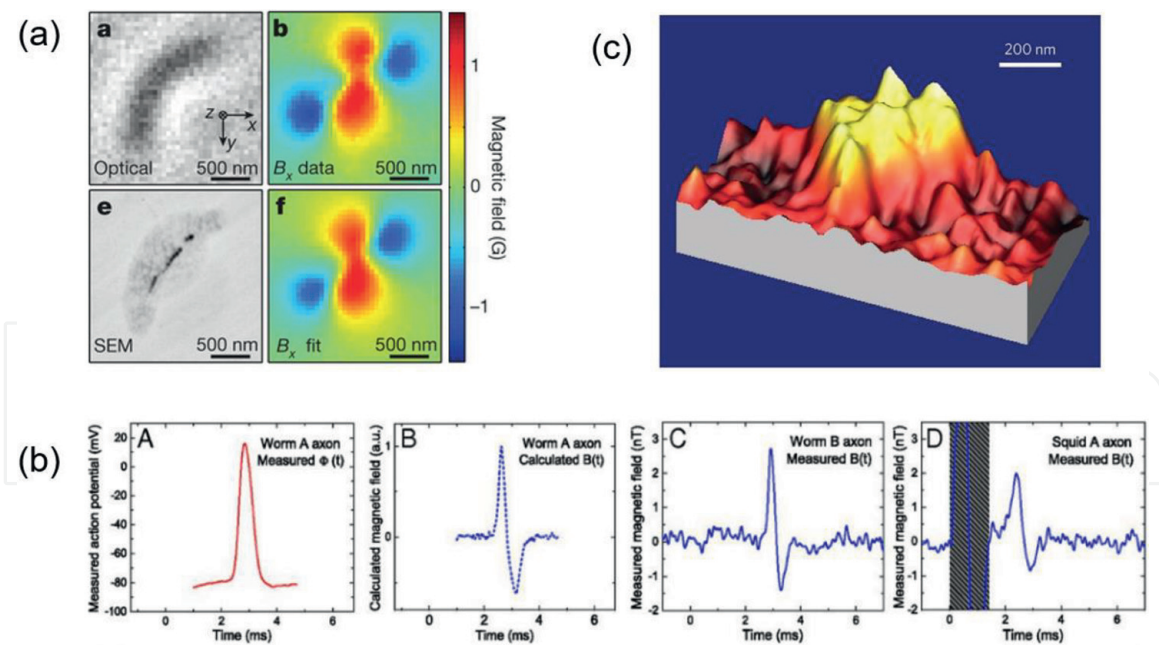
Figure 13.
Examples of magnetic sensing and imaging on biological samples. (a) Magnetic imaging on a single magnetotactic bacterium. Reprint with permission from [32] Copyright (2013) Nature (b) sensing of induced magnetic field due to the action potential in an axon. Reprint with permission from [34] Copyright (2016) Proceedings of the National Academy of Sciences (c) MRI imaging of a particle of poly(methyl methacrylate) (PMMA). Reprint with permission from [37] Copyright (2015) Nature Nanotechnology.

beam, total internal reflection fluorescence (TIRF) technique is typically adopted [32]. With the TIRF configuration, the excitation laser from the backside of the diamond is totally reflected at the interface between the diamond and the sample and is only illuminated onto the NV ensembles.

Figure 13a shows an example of the wide field-of-view magnetic imaging on biological samples e.g. bacteria called magnetotactic bacteria (MTB) [32]. MTB contain magnetic nano-particles in the body forming one dimensional chain that and are aligned along the external magnetic field. The diamond wide field-of-view optics successfully maps the stray field produced by a single MTB and identifies orientations of the magnetic chains from the field distribution.. Motivated by this work, scientists try to identify cancer cells among normal cells by selectively dosing magnetic nano-particles into the target cells and imaging the resulting magnetic field [33].

Owing to the capability of bio-imaging, the NV center gets increasing attentions in the field of neural science. Since neurons communicate each other via the motions of ions, it can be viewed as current flows in a conducting wire which produces magnetic field around it. By mapping the induced magnetic field with the NV center, therefore, one can study brain activities in the neural networks. As a first step toward this goal, recent experiment successfully demonstrates detection of magnetic field due to the action potential along an axon (**Figure 13b**) [34]. The NV center is also used to probe nuclear magnetic resonance (NMR) signal from a single protein [35] which opens up the possibilities of MRI at the nanometer-scale [37] (**Figure 13c**).

5. Conclusions

In this chapter, we introduce the diamond NV center as a novel magnetometer satisfying high magnetic field sensitivity and high spatial resolution. We review the

basic working principles of sensing dc and ac magnetic field and discuss two imaging applications which are based on scanning magnetometry and wide field-of-view optics techniques. The excellent properties of NV centers such as sub-nanotesla sensitivity, nanometer-scale resolution, gigahertz range of detection bandwidth, wide range of the operation temperature, non-toxic and bio-friendly host material position the NV center as a unique tool of sensing and imaging microscopic magnetic phenomena. Improving sensing protocols and imaging techniques is on-going efforts in this field. In conclusion, the novel magnetometer introduced in this chapter has a promising potential to be used in various research fields particularly solid-state physics and life science.

Acknowledgements

Author details

Myeongwon Lee, Jungbae Yoon and Donghun Lee*
Department of Physics, Korea University, Seoul, Republic of Korea

*Address all correspondence to: donghun@korea.ac.kr

IntechOpen

References

[1] Soaldin NA. Magnetic materials. 2nd ed. Fundamentals and Applications. Cambridge: Cambridge University Press; 2010. pp. 177–188. ISBN-13: 978–0521886697

[2] Shenton ME, Hamoda HM, Schneiderman JS, Bouix S, Pasternak O, Rathi Y, et al. A review of magnetic resonance imaging and diffusion tensor imaging findings in mild traumatic brain injury. Brain Imaging and Behavior. 2012;**6**(2):137-192. DOI: 10.1007/s11682-012-9156-5

[3] Hsieh D, Qian D, Wray L, Xia Y, Hor YS, Cava RJ, et al. A topological Dirac insulator in a quantum spin hall phase. Nature. 2008;**452**:970-974. DOI: 10.1038/nature06843

[4] Eerenstein W, Mathur ND, Scott JF. Multiferroic and magnetoelectric materials. Nature. 2006;**442**:759-765. DOI: 10.1038/nature05023

[5] Nagaosa N, Tokura Y. Topological properties and dynamics of magnetic skyrmions. Nature Nanotechnology. 2013;**8**:899-911. DOI: 10.1038/NNANO.2013.243

[6] Kuhn K, Kenyon C, Kornfeld A, Liu M, Maheshwari A, Shih W, et al. Managing process variation in Intel's 45 nm CMOS technology. Intel Technology Journal. 2008;**12**:93-109. DOI: 10.1535/itj.1202

[7] Parkin S, Jiang X, Kaiser C, Panchula A, Roche K, Samant M. Magnetically engineered spintronic sensors and memory. Proceedings of the IEEE. 2003; **91**:661-680. DOI: 10.1109/JPROC.2003.811807

[8] Rugar D, Budakian R, Hamin HJ, Chui BW. Single spin detection by magnetic resonance force microscopy. Nature. 2004;**430**:329-332. DOI: 10.1038/nature02658

[9] Schoelkopf RJ, Wahlgren P, Kozhevnikov AA, Delsing P, Prober DE. The radio-frequency single-electron transistor (RF-SET): A fast and ultrasensitive electrometer. Science. 1998;**280**:1238-1242. DOI: 10.1126/science.280.5367.1238

[10] Aassime A, Johansson G, Wendin G, Schoelkopf RJ, Delsing P. Radio-frequency single-electron transistor as readout device for Qubits: Charge sensitivity and Backaction. Physical Review Letters. 2001;**86**:3376-3379. DOI: 10.1103/PhysRevLett.86.3376

[11] Hasselbach K, Veauvy C, Mailly D. MicroSQUID magnetometry and magnetic imaging. Physica C. 2000;**332**: 140-147. DOI: 10.1016/S0921-4534(99)00657-7

[12] Oral A, Bending SJ. Real-time scanning Hall probe microscopy. Applied Physics Letters. 1996;**69**: 1324-1326. DOI: 10.1063/117582

[13] Wiesendanger R. Spin mapping at the nanoscale and atomic scale. Reviews of Modern Physics. 2009;**81**:1495-1550. DOI: 10.1103/RevModPhys.81.1495

[14] Hartmann U. Magnetic force microscopy. Annual Review of Materials Science. 1999;**29**:53-87. DOI: 10.1146/annurev.matsci.29.1.53

[15] Childress L, Hanson R. Diamond NV centers for quantum computing and quantum networks. MRS Bulletin. 2013; **38**:134-138. DOI: 10.1557/mrs.2013.20

[16] Taylor JM, Cappellaro P, Childress L, Jiang L, Budker D, Hemmer PR, et al. High-sensitivity diamond magnetometer with nanoscale resolution. Nature Physics. 2008;**4**: 810-816. DOI: 10.1038/nphys1075

[17] Rondin L, Tetienne JP, Rohart S, Thiaville A, Hingant T, Spinicelli P, et al.

Stray-field imaging of magnetic vortices with a single diamond spin. Nature Communications. 2013;**4**:1-5. DOI: 10.1038/ncomms3279

[18] Schrhagl R, Chang K, Loretz M, Degen CL. Nitrogen-vacancy centers in diamond: Nanoscale sensors for physics and biology. Annual Review of Physical Chemistry. 2014;**65**:83-105. DOI: 10.1146/annurev-physchem-040513-103659

[19] Lesik M, Spinicelli P, Pezzagna S, Happel P, Jacques V, Salord O, et al. Maskless and targeted creation of arrays of colour centres in diamond using focused ion beam technology. Physica Status Solidi (a). 2013;**210**:2055-2059. DOI: 10.1002/pssa.201300102

[20] Bar-Gill N, Pham LM, Jarmola A, Budker D, Walsworth RL. Solid-state electronic spin coherence time approaching one second. Nature Communications. 2013;**4**:1743. DOI: 10.1038/ncomms2771

[21] Wolf T, Neumann P, Nakamura K, Sumiya H, Ohshima T, Isoya J, et al. Subpicotesla diamond magnetometry. Physical Review X. 2015;**5**:041001. DOI: 10.1103/PhysRevX.5.041001

[22] Degen CL, Reinhard F, Cappellaro P. Quantum sensing. Reviews of Modern Physics. 2017;**89**:035002. DOI: 10.1103/RevModPhys.89.035002

[23] Dovzhenko Y, Casola F, Schlotter S, Zhou TX, Büttner F, Walsworth RL, et al. Magnetostatic twists in room-temperature skyrmions explored by nitrogen-vacancy center spin texture reconstruction. Nature Communications. 2018;**9**:2712. DOI: 10.1038/s41467-018-05158-9

[24] Thiel L, Rohner D, Ganzhorn M, Appel P, Neu E, Müller B, et al. Quantitative nanoscale vortex imaging using a cryogenic quantum magnetometer. Nature Nanotechnology. 2016;**11**:677-681. DOI: 10.1038/nnano.2016.63

[25] Pelliccione M, Jenkins A, Ovartchaiyapong P, Reetz C, Emmanouilidou E, Ni N, et al. Scanned probe imaging of nanoscale magnetism at cryogenic temperatures with a single-spin quantum sensor. Nature Nanotechnology. 2016;**11**:700-705. DOI: 10.1038/nnano.2016.68

[26] Tetienne JP, Hingant T, Kim JV, Diez LH, Adam JP, Garcia K, et al. Nanoscale imaging and control of domain-wall hopping with a nitrogen-vacancy center microscope. Science. 2014;**344**:1366-1369. DOI: 10.1126/science.1250113

[27] Lee M, Jang B, Yoon J, Mathpal MC, Lee Y, Kim C, et al. Magnetic imaging of a single ferromagnetic nanowire using diamond atomic sensors. Nanotechnology. 2018;**29**:405502. DOI: 10.1088/1361-6528/aad2fe

[28] Tetienne JP, Dontschuk N, Broadway DA, Stacey A, Simpson DA, Hollenberg LCL. Quantum imaging of current flow in graphene. Science Advances. 2017;**3**:e1602429. DOI: 10.1126/sciadv.1602429

[29] Pelliccione M, Myers BA, Pascal LMA, Das A, Bleszynski Jayich AC. Two-dimensional nanoscale imaging of gadolinium spins via scanning probe relaxometry with a single spin in diamond. Physical Review Applied. 2014;**2**:054014. DOI: 10.1103/PhysRevApplied.2.054014

[30] Zaiser S, Rendler T, Jakobi I, Wolf T, Lee S-Y, Wagner S, et al. Enhancing quantum sensing sensitivity by a quantum memory. Nature Communications. 2016;**7**:12279. DOI: 10.1038/ncomms12279

[31] Gross I, Akhtar W, Garcia V, Martínez LJ, Chouaieb S, Garcia K, et al. Real-space imaging of non-collinear

antiferromagnetic order with a single-spin magnetometer. Nature. 2017;**549**: 252-256. DOI: 10.1038/nature23656

[32] Le Sage D, Arai K, Glenn DR, DeVience SJ, Pham LM, Rahn-Lee L, et al. Optical magnetic imaging of living cells. Nature. 2014;**496**:486-489. DOI: 10.1038/nature12072

[33] Glenn DR, Lee K, Park H, Weissleder R, Yacoby A, Lukin MD, et al. Single-cell magnetic imaging using a quantum diamond microscope. Nature Methods. 2015;**12**:1-5. DOI: 10.1038/nmeth.3449

[34] Barry JF, Turner MJ, Schloss JM, Glenn DR, Song Y, Lukin MD, et al. Optical magnetic detection of single-neuron action potentials using quantum defects in diamond. Proceedings of the National Academy of Sciences. 2016;**113**: 14133-14138. DOI: 10.1073/pnas.1601513113

[35] Lovchinsky I, Sushkov AO, Urbach E, de Leon NP, Choi S, De Greve K, et al. Nuclear magnetic resonance detection and spectroscopy of single proteins using quantum logic. Science. 2016;**351**: 836-841. DOI: 10.1126/science.aad8022

[36] Maze JR. Quantum Manipulation of Nitrogen-Vacancy Centers in Diamond: From Basic Properties to Applications. Harvard University; 2010. Available from ProQuest Dissertations & Thesis Global: https://search.proquest.com/docview/612776202?accountid=14558 [Accessed: 2019-02-01]

[37] Rugar D, Mamin HJ, Sherwood MH, Kim M, Rettner CT, Ohno K, et al. Proton magnetic resonance imaging using a nitrogen-vacancy spin sensor. Nature Nanotechnology. 2015;**10**: 120-124. DOI: 10.1038/nnano.2014.288

[38] Vengalattore M, Higbie JM, Leslie SR, Guzman J, Sadler LE, Stamper-Kurn DM. High-Resolution Magnetometry with a Spinor Bose-Einstein Condensate.

Physical Review Letters. 2017;**98**: 200801. DOI: 10.1103/PhysRevLett.98.200801

[39] Faley MI, Poppe U, Urban K, Paulson DN, Fagaly RL. A new generation of the HTS multilayer DC-SQUID magnetometers and gradiometers. Journal of Physics: Conference Series. 2006;**43**:1199-1202. DOI:: 10.1088/1742-6596/43/1/292

[40] Baudenbacher F, Fong LE, Holzer JR, Radparvar M. Monolithic low-transition-temperature superconducting magnetometers for high resolution imaging magnetic fields of room temperature samples. Applied Physics Letters. 2003;**82**:3487-3489. DOI: 10.1063/1.1572968

[41] SANDHU A, Okamoto A, Shibasaki I, Oral A. Nano and micro Hall-effect sensors for room-temperature scanning hall probe microscopy. Microelectronic Engineering. 2004;**73-74**:524-528. DOI: 10.1016/j.mee.2004.03.029

[42] Sandhu A, Kurosawa K, Dede M, Oral A. Japanese Journal of Applied Physics. 2004;**43**:777-778. DOI: 10.1143/JJAP.43.777

[43] Vengalattore M, Higbie JM, Leslie SR, Guzman J, Sadler LE, Stamper-Kurn DM. High-Resolution Magnetometry with a Spinor Bose-Einstein Condensate. Physical Review Letters. 2007;**98**: 200801. DOI: 10.1103/PhysRevLett.98.200801

[44] Shah V, Knappe S, Schwindt PDD, Kitching J. Subpicotesla atomic magnetometry with a microfabricated vapour cell. Nature Photonics. 2007;**1**: 649-652. DOI: 10.1038/nphoton.2007.201